

Video Article

Fused Filament Fabrication (FFF) of Metal-Ceramic Components

Johannes Abel¹, Uwe Scheithauer¹, Thomas Janics², Stefan Hampel², Santiago Cano³, Axel Müller-Köhn¹, Anne Günther¹, Christian Kukla⁴, Tassilo Moritz¹

¹Fraunhofer Institute for Ceramic Technologies and Systems IKTS

²HAGE Sondermaschinenbau GmbH & Co KG

³Institute of Polymer Processing, Montanuniversitaet Leoben

⁴Industrial Liaison Department, Montanuniversitaet Leoben

Correspondence to: Johannes Abel at johannes.abel@ikts.fraunhofer.de

URL: <https://www.jove.com/video/57693>

DOI: [doi:10.3791/57693](https://doi.org/10.3791/57693)

Keywords: Engineering, Issue 143, Additive Manufacturing, Fused Filament Fabrication, Ceramic, Metal, Multi-Material, Zirconia, Stainless steel, Composite, FFF, FDM, T3DP

Date Published: 1/11/2019

Citation: Abel, J., Scheithauer, U., Janics, T., Hampel, S., Cano, S., Müller-Köhn, A., Günther, A., Kukla, C., Moritz, T. Fused Filament Fabrication (FFF) of Metal-Ceramic Components. *J. Vis. Exp.* (143), e57693, doi:10.3791/57693 (2019).

Abstract

Technical ceramics are widely used for industrial and research applications, as well as for consumer goods. Today, the demand for complex geometries with diverse customization options and favorable production methods is increasing continuously. With fused filament fabrication (FFF), it is possible to produce large and complex components quickly with high material efficiency. In FFF, a continuous thermoplastic filament is melted in a heated nozzle and deposited below. The computer-controlled print head is moved in order to build up the desired shape layer by layer. Investigations regarding printing of metals or ceramics are increasing more and more in research and industry. This study focuses on additive manufacturing (AM) with a multi-material approach to combine a metal (stainless steel) with a technical ceramic (zirconia: ZrO₂). Combining these materials offers a broad variety of applications due to their different electrical and mechanical properties. The paper shows the main issues in preparation of the material and feedstock, device development, and printing of these composites.

Video Link

The video component of this article can be found at <https://www.jove.com/video/57693/>

Introduction

According to ISO/ASTM, additive manufacturing (AM) is the general term for technologies that create physical objects based on a geometrical representation by successive addition of material¹. Hence, these technologies offer the possibility of manufacturing components with extremely complex geometry, which cannot be attained by any other shaping technique known to the authors.

Ceramic materials have been studied since the early development of the different AM technologies in the past quarter century^{2,3}; however, additive manufacturing of ceramic components is not state of the art in contrast to additive manufacturing of polymer or metal components. Several overviews about the AM technologies used for ceramic components are given by Chartier *et al.*⁴, Travitzky *et al.*⁵ and Zocca *et al.*⁶, which can be classified according to the state of the material that is used - powder materials, liquid materials, and solid materials^{4,5} or according to the kind of material deposition and solidification⁶. AM devices are available that allow the additive manufacturing of dense and high-quality ceramic components with the desired properties for most applications^{7,8,9,10,11}.

Production of ceramic components requires complex processing, and this has stalled progress in the AM of ceramics. Nevertheless, ceramic components are indispensable for special consumer goods and medical devices, and AM opens up new horizons for the fabrication of novel components with "impossible" geometries¹². For technical ceramic components, a subsequent thermal treatment of the manufactured components is required since the AM shaping of ceramics requires the use of powders suspended in organic binders that need to be removed (*i.e.*, debinding) before the powder is fused together (*i.e.*, sintering).

The AM of multi-material or multi-functional components combines the benefits of AM and functionally graded materials (FGM)¹³ into ceramic-based 4D-components¹⁴. Material hybrids allow property combinations such as electrically conductive/insulating, magnetic/non-magnetic, ductile/hard or different colorations. Hybrid components can exhibit sensor or actuator functions known from MEMS (micro electromechanical systems)¹⁵ as well. Furthermore, metal/ceramic composites can complement joining ceramic parts into machines since conventional weldable steel partners can be used.

The European Project cerAMufacturing (EU-Project CORDIS 678503) is developing AM technologies for single material components as well as a completely new approach for AM of multi-material components, which will allow serial production of customized and multifunctional components for various applications¹². Three different suspension-based AM techniques are qualified to allow the AM of ceramic-ceramic as well as metal-ceramic components. The utilization of suspension-based AM techniques promises improved component performance in comparison to powder-

based methods. Because the particle distribution of the powder in a suspension is more homogeneous and more compact than in a powder bed, these shaping methods yield higher green densities, which result in sintered components with dense microstructures and low surface roughness levels¹².

Along with lithography-based ceramic manufacturing (LCM)^{7,8,9,10,11,16,17}, fused filament fabrication (FFF) and thermoplastic 3D-printing (T3DP)^{12,14,18} are being developed. FFF and T3DP are more suitable for the AM of multi-material components than LCM because of the selective deposition and solidification of the certain material instead of the pure selective solidification of material deposited all over the entire layer¹⁴.

An additional benefit of FFF and T3DP compared to LCM is the use of thermoplastic binder systems instead of photo-curing polymers. The binder system enables the processing of powders independent of their optical properties such as absorption, emission and reflection of electromagnetic waves, e.g., dark and bright materials (in visible range), which is necessary for the production of metal-ceramic components^{19,20}. Furthermore, low investment is required for the FFF equipment since a large variety of standard devices are available. This technique becomes economical due to the high material efficiency and the recyclable materials. Finally, FFF is easy to upscale for large parts since the process relies on moving print head on axes.

This paper presents the first results of manufacturing metal-ceramic composites using FFF. Additionally, the technical combination of FFF and T3DP units is presented, although it is still under development. In the FFF process, filaments of thermoplastic polymers are melted and selectively extruded by the action of two counter rotating elements. Once the material is extruded through the nozzle, it solidifies by cooling, enabling the production of components layer-by-layer. To produce final ceramic and metallic components, a variant of the process has been developed^{21,22,23,24,25,26}. The polymeric compounds, known as binders, are highly filled with a ceramic or metallic powder. Once the shaping of the components has been conducted using the conventional FFF approach, two additional steps are required. First, the polymeric components must be completely removed from the specimens in the debinding stage, generating a structure with numerous micro-sized pores. To attain the final properties, the powder compacts are subsequently sintered at a temperature below the melting point of the material. Using this approach, the production of materials such as silicon nitride, fused silica, piezoelectric ceramics, stainless steels, tungsten carbide-cobalt, alumina or titanium dioxide^{23,24,25} has been successfully conducted elsewhere.

The use of highly-filled polymeric filaments and the characteristic of the process impose certain requirements in the materials²¹. Good compatibility must be provided between the thermoplastic binder components and the powder, which must be homogeneously distributed using compounding techniques at temperatures above the melting point of the organic binder components, such as kneading or shear rolling. Since the solid filament has to act as a piston in the print head to push the molten material, a high stiffness and a low viscosity are required to enable the extrusion of the material through the nozzle with typical diameters ranging from 0.3 to 1.0 mm. Meanwhile, the material must possess enough flexibility and strength to be shaped as a filament that can be spooled. To combine all these properties while having a high load of powder, different multi-component binder systems have been developed^{21,22,26}.

In addition to the use of adequate binder formulation, a new driving system has been employed in this work. Commonly, toothed drive wheels are used to push the filament through the nozzle. These teeth can damage the brittle filament. In order to reduce the mechanical requirements of the filaments and increase the extrusion pressure during the FFF process, the conventional FFF system of toothed drive wheels was replaced by a special dual belt system. High friction and guidance is generated due to the length, the shape, and the special rubber coating of the belts. The most important issue was preventing any buckling of the filament through the print head. The filament must be guided all the way to the nozzle, no free space is allowed, and the necessary transitions between the components have to be considered.

After leaving the feeding unit, the filament enters the nozzle unit. The main goals were designed temperature management and gapless guidance. The developed print head is shown in **Figure 1**.

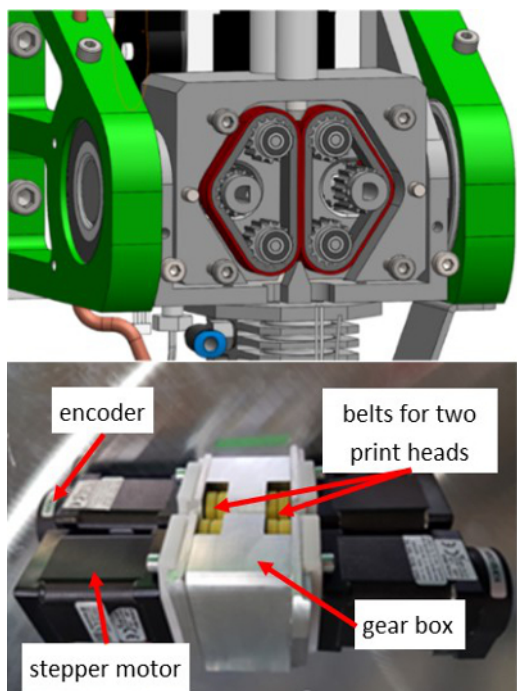


Figure 1: CAD model of the new belt drive unit (top) and image of the real unit (bottom). [Please click here to view a larger version of this figure.](#)

Another big challenge to be addressed for the production of metal-ceramic components is the selection of powders that allow co-processing during the thermal treatment (comparable coefficient of thermal expansion (CTE), temperature regimes, and atmosphere) and particularly the adjustment of the shrinkage behavior of both materials during the sintering step. In this work, an attempt is made to combine zirconia and modified stainless steel 17-4PH since they have a comparable CTE (approx. $11 \times 10^{-6}/K$) and can be sintered at the same conditions (reducing hydrogen atmosphere, sintering temperature: 1350 - 1400 °C). However, for adjusting the shrinkage behavior, a special milling procedure for the metallic powder is required^{19,20}.

Protocol

1. Materials Used

1. Selection of the binder components
 1. Select the binder system according to the criteria of highly filled compounds (powder content of approximately 50 vol. %) defined for FFF: high mechanical strength, enough stiffness, low viscosity and flexibility for spooling. A drastic reduction of the flexibility and the increase of the viscosity can be expected by a high solid loading.
NOTE: In this study, a multi-component binder system was employed. The majority of the components consisted of a thermoplastic elastomer to improve flexibility and strength. A functionalized polyolefin was included as a backbone to improve the adhesion with the powder. Finally, stearic acid (circa 5 vol. %) was incorporated as a surfactant for good dispersion of the powders. Due to confidentiality reasons, more information cannot be disclosed.
2. Selection of powders
 1. Choose a suitable powder couple for the multi-material approach. For co-processing of a ceramic and a metal powder, choose materials with the same coefficient of thermal expansion (CTE) and the same shrinkage behavior during sintering in the same sintering atmosphere.
 2. Select the specific ceramic grade. Choose tetragonal yttria-stabilized zirconia due the CTE and sintering temperature being comparable to special stainless steels as well as the high toughness and flexural strength of this ceramic material. Use zirconia powder with a specific surface area of $7 \pm 2 \text{ m}^2/\text{g}$ and a particle size of $d_{50} = 0.5 \mu\text{m}$.
 3. Select the specific metal grade. Use stainless steel powder as the conductive and ductile metallic material. The material must have a comparable CTE and a similar range of sintering temperatures to those of the zirconia under a protective hydrogen atmosphere.
3. Adjustment of sintering behavior
 1. To attain a stress-free co-sintering, adjust the temperature dependent strain behavior (shrinkage due to sintering and thermal expansion) of both powder types. Since the zirconia powder used has high surface energy due to the fine particles, modify the stainless steel powder by refining the comparatively large metal particles and increasing the dislocation density by deformation of the atomic lattice.
NOTE: First during attrition milling, the spherical steel particles are re-shaped into thin and brittle flakes with an extremely high dislocation density. Secondly during the high energy milling step (planetary ball milling, PBM), the brittle flakes will be broken into very

fine-grained particles with an increased sintering ability. In this way, increased sintering activity of the metallic powder can be reached and the shrinking curve could be adjusted to the curve of zirconia, showing only small differences^{19,20}.

1. Apply attrition milling (180 min) to the spherical stainless steel particles to re-shape into thin and brittle flakes.
2. Perform planetary ball milling (240 min) to break the brittle flakes into very fine-grained particles with a decreased aspect ratio but an increased sintering ability.

4. Evaluate the adjustment success

1. Use a rod or optical dilatometer to measure the shrinkage behavior of suitable material compacts and compare the results. Use the volumetric powder content of both materials is the same and apply the same measurement (heating rates, atmosphere, maximum temperature, dwell time).
2. If there is a high mismatch in sintering behavior, adjust the milling parameters of the stainless steel powder. Finer powders will lead to a lower sinter starting temperature. A longer attrition milling time will lead to higher dislocation energies and higher shrinkage. Planetary milling leads to spattered powder, which is applicable in polymer compounds.

NOTE: The success of the adjustment is influenced by the raw materials. Optimization must be conducted. A shifting of the sintering curves can also be generated by fractioning the powders. Fine powder fractions tend to begin sintering at lower temperatures.

2. Filament Production

1. Feedstock preparation

NOTE: For the preparation of the zirconia feedstock, dry the powder to reduce its tendency to agglomerate²⁷. Dry the material at 80 °C in a vacuum oven for a minimum of 1 hour.

1. Pre-compound the material in a roller rotors mixer for 30 minutes at 60 rpm.
 1. Ensure that the temperature is high enough to melt all the binder components. Introduce the binder components and wait until melting. Feed the powder in 5 consecutive loads every 5 min.
 2. At the end of the process, extract the material from the chamber in small pieces to facilitate step 2.1.2.

NOTE: For both materials, powder contents of 47 vol. % were realized within the thermoplastic feedstocks.

2. Granulate or pelletize the solid material after cooling to room temperature.
 1. When a cutting mill is employed, introduce the material pieces gradually. Wait until the pieces inside are granulated to introduce the next ones.
 2. At the exit of the grinding chamber, use a sieve with 4 x 4 mm squared perforations to get granules of adequate size. This procedure is necessary for a continuous feeding of the twin screw extruder or shear roller (step 2.1.3).
3. Compound the material at high shear rates to improve the dispersion, e.g., in a co-rotating twin screw extruder (TSE) or in a shear roll extruder. Collect the material with a conveyor belt and cool it down to room temperature.

NOTE: In this study, a co-rotating twin screw extruder was used. The screw rotation speed was set to 600 rpm and a temperature profile from 170 °C in the feeding zone until 210 °C in the die was defined.
4. Granulate or pelletize the solid material after cooling to room temperature. Use the procedure of 2.1.2 or pelletize the material at the end of the conveyor belt with a pelletizer. If necessary, repeat the process until the pellets have a length equal or smaller than 4 mm.

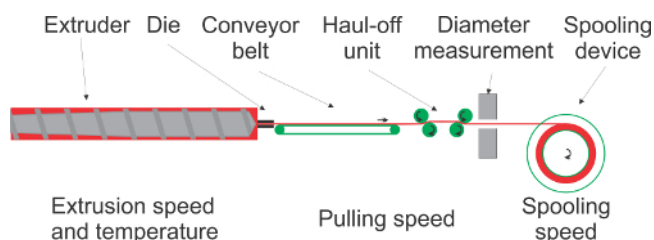


Figure 2: Filament production line. The material is extruded on a controlled manner by the regulation of the extrusion speed and temperature. Afterwards, it is collected and driven by a conveyor belt and haul-off unit. The filament diameter is measured and if the values are within the desired range, the filament is spooled. To regulate the filament dimensions, the pulling and spooling speeds must be progressively adjusted. [Please click here to view a larger version of this figure.](#)

2. Filament extrusion

NOTE: **Figure 2** shows a scheme of the manufacturing process for filament preparation and the variable parameters that define the filament diameter at the bottom. The filament is collected by a conveyor belt and pulled by the action of two pairs of counter rotating rollers. The diameter and ovality values are measured in a laser measurement device, and the process parameters are adjusted to regulate the filament geometry. The material is finally stored on spools. The production of filaments with a constant range of dimensions is critical for the repeatability of the process, since the volume flow in FFF is dependent of the filament geometry.

1. Extrude the material at 30 rpm at a temperature above the melting point of the binder components. For a good control of the pressure and filament quality, use a single screw extruder with a nozzle diameter of at least 1.75 mm.

NOTE: For small quantities of material, a high pressure capillary rheometer can be employed in the material development phase. Nevertheless, a poor dimensional quality of the filament can be expected.

NOTE: Steps 2.1 and 2.2.1 can be combined in an adequate twin screw extrusion process.
2. Collect the extruded material. Use a conveyor belt to collect and cool down the extruded material. Air or water cooling elements can be required when using high extrusion speeds.

3. Measure and control the dimensions of the filament. For a particular extrusion speed, progressively regulate the conveyor belt and pulling speeds to adjust the dimensions of the filament (decrease the conveyor and pulling speeds for a higher diameter). Produce filaments with a diameter range of 1.70 to 1.80 mm and ovality smaller than 0.10 mm.
NOTE: The ovality value is defined as the difference between the maximum and minimum diameters. For a perfectly round filament, an ovality of zero must be obtained.
4. Spool the material. An additional spooling unit (**Figure 2**) can be placed at the end of the conveyor belt for automatic spooling.

3. Additive Manufacturing of Green Components

1. Investigation of optimum process parameters
 1. Before printing, use commercial slicing software. This software can be applied to set up the printing parameters and to generate the g-code for the printing device out of a 3D-CAD model.
 2. For printing, consider the following essential parameters:
 - bed temperature for bed adhesion
 - print speed of different materials
 - varying print temperature for constant material flow
 - control of cooling fan to support solidification of printed strand
 - print temperature for improved adhesion between layers
 - retraction parameters to avoid oozing and using a "prime pillar"
 - varying material flow to assure same strand width of different materials
2. AM of test components
 1. Perform AM of green samples with a commercial 3D printer (see **Table of Materials**). Manufacture single-material test components before printing multi-material components.
 1. Correct any possible misalignment of the nozzles in the printer software before manufacturing multi-material components.
 2. Single component manufacturing
 1. Load print head 1 with the zirconia filament and print head 2 with the stainless steel-filament. For both filaments, use a print head speed of 10 mm/s and print bed temperature of 20 °C. Set the print head temperature of zirconia to 220 °C and stainless steel to 240 °C.
NOTE: As a first test geometry sample, cuboids were manufactured for the single materials and different sandwich setup has been chosen for the multi-material component. All green components had final dimensions of 15 mm x 15 mm and varied thickness 1 - 3 mm and were manufactured with a layer thickness of 0.25 mm. The print head temperature can be varied to achieve the desired flowability of the feedstocks. Raising the temperature leads to a reduction of the viscosity. The optimal printing temperatures of the two materials may differ.
 3. Multi-material manufacturing
 1. Manufacture multi-material components by alternating with two or three different layers, e.g., 1 mm stainless steel / 1 mm zirconia / 1 mm stainless steel or 1 mm zirconia / 1 mm stainless steel / 1 mm zirconia.
NOTE: In multi-component printing, it can be very helpful to use a "prime pillar" for sharp and precise material transitions. When changing the print head, a few millimeters of filament are needed until the material fills the used nozzle to be extruded, leading to gaps. Therefore, the appearance of the part is not as good as it could be. To avoid this behavior, print the "prime pillar" beside the part, this can be set in the software. A layer of the prime pillar (rectangular tower, **Figure 3**) will be printed first when changing the nozzle, to ensure that the nozzle is primed and ready to print before continuing with the part layers.
 4. Optimization of the manufacturing
 1. Use an "ooze-shield" if needed; this is a printed thin wall around the component (**Figure 4**). After the print head changes for the second component outside the part, have the nozzle cross this wall when it moves from the tower. All adhering material will be peeled off from the nozzle at this shield and the precision of material deposition on the part to be printed can be increased.
NOTE: Further optimizations regarding the achievable quality are possible by finer adjustments of the flow, the extrusion width, and the extrusion multiplier, assuming that the diameter of the filament is constant.

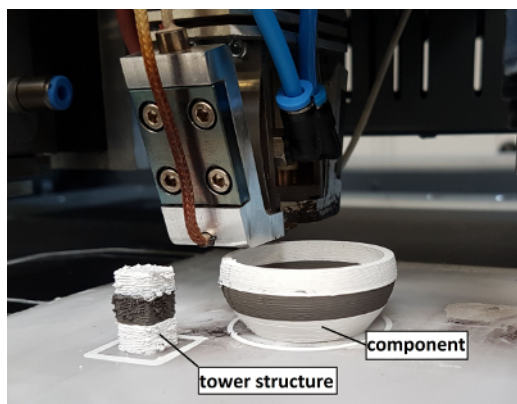


Figure 3: Manufacturing process for metal-ceramic component with tower structure. [Please click here to view a larger version of this figure.](#)



Figure 4: Virtual print of a component with surrounding ooze-shield. [Please click here to view a larger version of this figure.](#)

4. Debinding and Sintering of Components

1. Carry out debinding in two consecutive steps. First, perform solvent extraction, and then thermal treatment to decompose the residual binder components.
 1. Conduct solvent extraction with the printed green parts using cyclohexane at 60 °C. Cover the samples with enough cyclohexane and treat them for 8 h. Consider fire safety aspects when carrying out this step. A soluble binder content of about 7-9 wt. % will be removed here.
NOTE: Applying a solvent extraction leads to reduced bloating effects during subsequent thermaldebinding.
 2. Perform thermal debinding in a debinding furnace in an argon atmosphere in order to protect the materials from reduction (occurred under nitrogen atmosphere) or oxidation. Use a maximum temperature of 440 °C and different heating rates between 5 °C/h and 150 °C/h.
 1. To characterize or optimize the debinding behavior of both feedstocks, apply a thermogravimetric analysis under nitrogen flow up to 600 °C to evaluate appropriate heating rates.
2. Carry out sintering in a reducing atmosphere of 80% argon and 20% hydrogen in a high-temperature tungsten furnace. Use heating rates between 3 °C/min and 5 °C/min to reach a maximum temperature of 1,365 °C. After a dwell time of 3 h, cool the kiln to room temperature.

Representative Results

The best fitting results for stainless steel sintering behavior were obtained with an attrition milling time of 180 minutes and a planetary ball mill (PBM) milling time of 240 minutes. **Figure 5** shows a SEM-image of the untreated powder (left), the deformed particles after the attrition milling (middle), and the chopped particles after the PBM milling step (right).

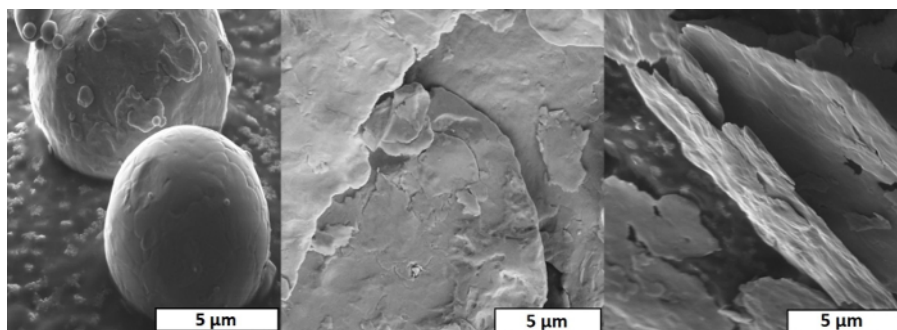


Figure 5: Untreated stainless steel $<38 \mu\text{m}</math> (D90) (left), stainless steel powder after attrition milling (middle), and stainless steel powder after PBM milling (right) Please click here to view a larger version of this figure.$

The sintering behavior of the initial and milled steel powder are compared with the sintering behavior of the zirconia powder in **Figure 6**, all measured with an optical dilatometer.

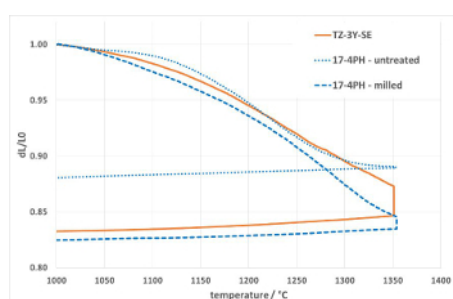


Figure 6: Dilatometric curves of the zirconia powder (TZ-3Y-SE) and the stainless steel powder (17-4PH) in the initial state and after a high-energy milling treatment of the stainless steel powder. Please click here to view a larger version of this figure.

The improvement of the feedstock mechanical properties in the high shear compounding step was characterized for the zirconia feedstock. A feedstock produced in a single compounding step of 75 min in a roller rotors mixer (RM) was compared with the one produced by the method described in the protocol. Filaments were extruded using a high pressure capillary rheometer with a die of 1.75 mm diameter, a piston speed of 1 mm/s and a temperature of 190 °C. The filaments were collected with a conveyor belt and tested with a universal tensile testing machine. At least 5 repetitions were conducted per material. **Figure 7** shows a comparison of both materials concerning the ultimate tensile strength (UTS), the elongation at UTS, and the secant modulus.

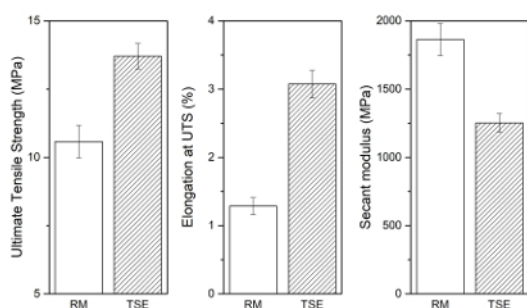


Figure 7: Influence of the compounding method in the mechanical properties of the zirconia feedstock. Feedstock was compounded in an internal roller mixer (RM) or in combination with a co-rotating twin screw step (TSE). The strength, flexibility and stiffness of filaments produced with a capillary rheometer were determined using the mean value and the correspondent standard deviation of the ultimate tensile strength (UTS), the elongation at UTS and the secant modulus, respectively. Please click here to view a larger version of this figure.

In **Figure 8**, the diameter values obtained during the production of the filaments made of zirconia (left) and stainless steel (right) feedstocks are presented. The diameter of the extruded filament was recorded during the production process via single-screw extrusion. For the zirconia filaments, a good control of the dimensions could be achieved with a mean diameter of 1.75 mm and a standard deviation of 0.02 mm. For the filaments containing the modified stainless steel powder, a higher variability of the average filament diameter was observed. A possible reason for this could be an inhomogeneous particle distribution within the feedstock resulting from the platelet-like shape of the metallic particles (**Figure 5**). In this case, a higher number of measurement points were found outside the desired range of $1.75 \text{ mm} \pm 0.05 \text{ mm}$, and the mean diameter value was 1.74 mm with a standard variation of 0.03 mm. For both types of filaments, the ovality values were considerably smaller than the 0.1 mm limit.

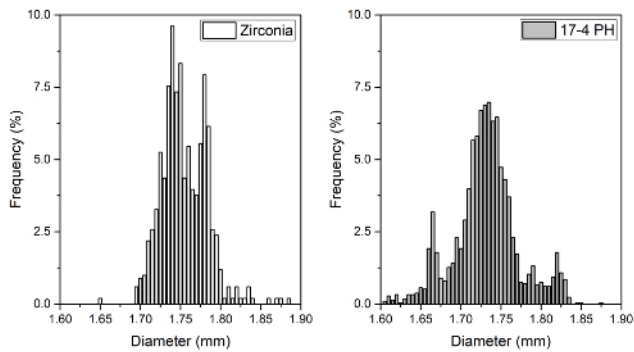


Figure 8: Histograms of the filament diameter for the studied materials. [Please click here to view a larger version of this figure.](#)

Figure 9 shows the suitable metal and zirconia filaments to manufacture green sandwich structures with the composition steel-zirconia-steel (left) as well as zirconia-steel-zirconia (right).

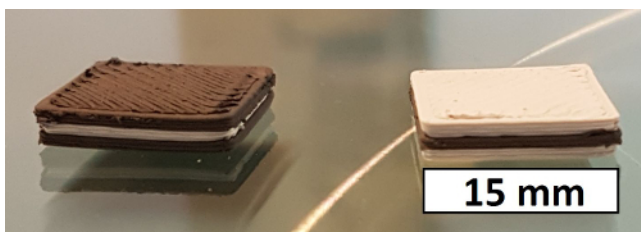


Figure 9: Green steel-zirconia-steel (left) and zirconia-steel-zirconia components (right) additively manufactured by FFF. [Please click here to view a larger version of this figure.](#)

Due to the similar binder system of both materials, it is possible to fuse certain layers to a monolithic composite part. A larger round shaped part with sharp transitions is shown in **Figure 10**.

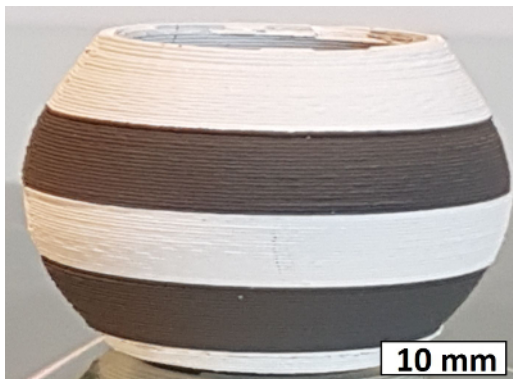


Figure 10: Structure with sharp transitions between Zirconia and stainless steel. [Please click here to view a larger version of this figure.](#)

Figure 11 shows other green single- and multi-material components that were further processed. **Figure 12** shows a pure zirconia sample on the left side, The middle shows a pure stainless steel sample, and finally a sintered and well joined steel-ceramic composite is pictured on the right side.

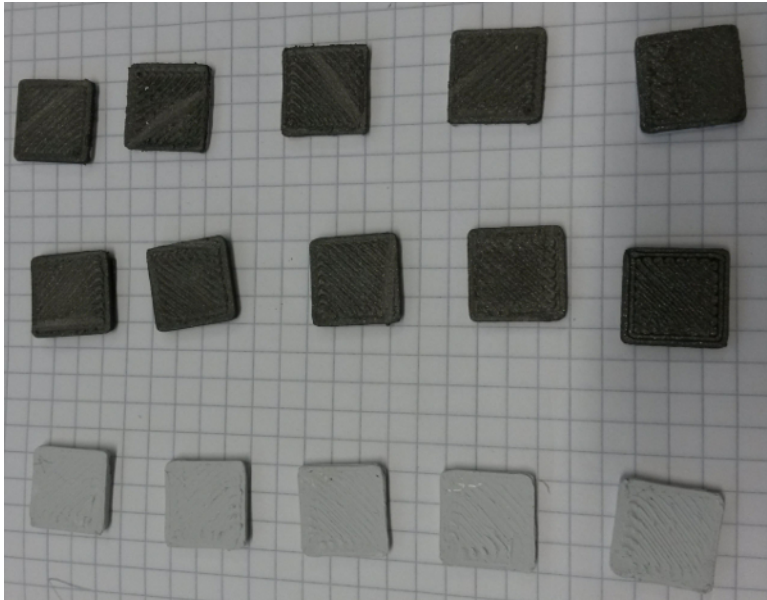


Figure 11: Green test samples manufactured by FFF; top: zirconia-steel-composites with stainless steel on top; middle: stainless steel; bottom: zirconia. Grid box 5 mm. [Please click here to view a larger version of this figure.](#)

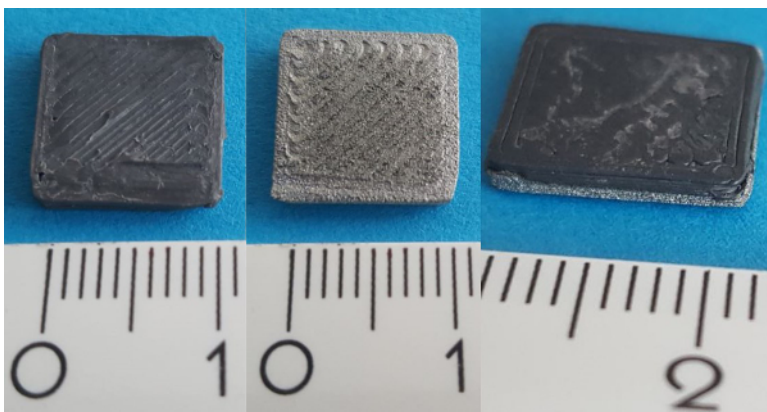


Figure 12: Sintered zirconia sample (left), sintered stainless steel sample (middle), and sintered zirconia-stainless steel-composite (right). All scales in mm. [Please click here to view a larger version of this figure.](#)

In **Figure 13**, a typical structure of FFF-components with crotches (or sub-perimeter) between two deposited filaments is shown, which resulted from an ordinary slicing (tool path) and the continuous way of material deposition.

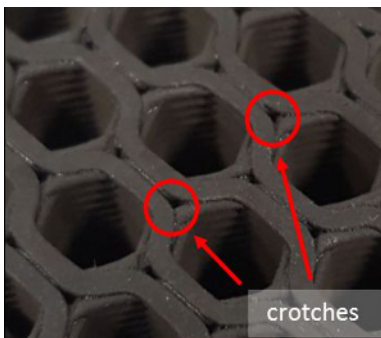


Figure 13: Typical structure of FFF-components resulting from slicing and continuous material deposition. [Please click here to view a larger version of this figure.](#)

By raising the extrusion multiplier in the slicing software, which leads to a higher volume deposition, the sub-perimeter can be reduced as well as by adapting the tool paths. Nevertheless, due to the high content of particles in the filaments, it is evident that the deposition behavior differs from ordinary printing of thermoplastics. Therefore, a software modification to close such defects is desirable.

After solvent debinding, thermal debinding and subsequent sintering, all the different samples showed no significant deformation or bloating. The sintered pure zirconia and stainless steel FFF specimens have a good geometrical stability both with and without compressive load and they do not buckle. The total mass loss was 14.8-14.9%, indicating complete debinding.

The metal-ceramic samples showed a good macroscopic adhesion of both materials. The mass loss after the sintering of the composites was found to be 14.1-14.4%, which also indicates a full debinding. Further analysis and process adjustments will follow. The electron microscope characterization of the composites is intended to provide insight into the quality of the composite. The desired formation of the composite has taken place successfully as shown in **Figure 14**.

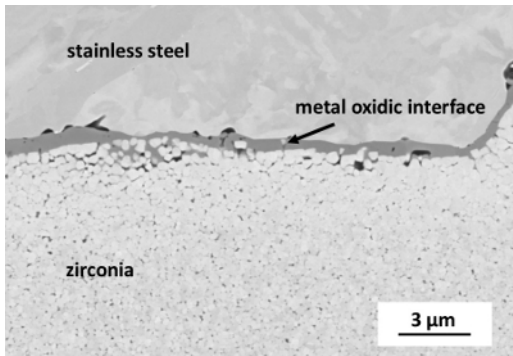


Figure 14: SEM Image of microstructure in the metal-ceramic interface showing the material joint. [Please click here to view a larger version of this figure.](#)

The results show that a promising approach to manufacture metal-ceramic composites using FFF generating electrical conductive and electrical isolating properties into one component. Furthermore, the implementation of ceramic parts into metallic environments becomes possible due to the good material bond and weldability of the stainless steel. Within the EU, project heating devices were manufactured by FFF containing an electrical conductive path made of stainless steel in a non-conductive ZrO_2 matrix. **Figure 15** shows the sintered samples. These multi-material components must be analyzed and tested in the future.

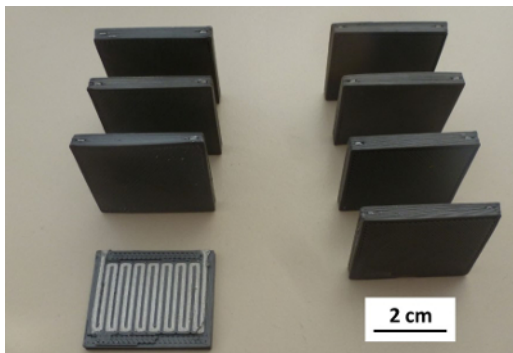


Figure 15: Sintered heating elements made of zirconia and stainless steel [Please click here to view a larger version of this figure.](#)

Figure 16 and **Figure 17** show the new print head with two FFF-printing heads and two T3DP-printing heads as CAD-model (**Figure 16**) as well as implemented in the FFF device (**Figure 17**). One challenge is controlling the output for both systems. For the micro dispensing units, the output is controlled by the frequency of a piezo-driven piston instead of the stepper motors speed for the belt drives within the FFF-printing heads. The interaction of both devices must be tested in the future.



Figure 16: CAD model of new print head with two FFF-printing heads and two T3DP-printing heads. [Please click here to view a larger version of this figure.](#)

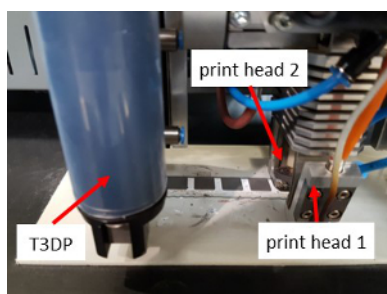


Figure 17: Image of new print head with two FFF-printing heads and one T3DP-printing head (left). [Please click here to view a larger version of this figure.](#)

Discussion

The zirconia and stainless steel used here are very suitable for the co-sintering of metal-ceramic components because of the comparable CTE, sintering temperature, and sintering atmosphere. The sintering behavior of the zirconia and the stainless steel feedstocks could be adjusted by the treatment of the stainless steel powder (**Figure 9**) successfully. By using the mentioned materials and methods, it is possible to manufacture macroscopic defect-free parts by FFF for the first time. To the authors' knowledge, no other comparable AM method is known to manufacture such parts except for T3DP^{19,20}. One application for metal ceramic components is shown in **Figure 17**, which is a heating element with an electrical conducting looped stainless steel in an isolating zirconia matrix.

One of the major challenges for the FFF of metallic and ceramic components is the dramatic increase of the stiffness and brittleness of the filaments due to the high solid content. Therefore, the selection of the right binder components was a key factor for the success of the project. In addition, the strength and flexibility of the filaments could be improved by the use of a high shear mixing technique (**Figure 7**). According to previous studies with highly filled systems²⁸, this improvement could be caused by a better powder dispersion and reduction of the agglomerates^{29,30}.

The investigation and adjustment of the extrusion, pulling and spooling speeds during the filament production process allowed the production of highly particle-filled filaments with the proper dimensions. Other parameters like the temperature distribution within the extruder as well as the use of cooling devices significantly influenced the filament quality and were chosen carefully.

Both filaments were processed in the FFF-device successfully. The adhesion between the feedstocks was found to be very good in the green state (**Figure 7-9**). Only some small unfilled volumes were visible, which are typically for a state of the art FFF process (**Figure 13**). To close these critical volumes with thermoplastic materials, the FFF-device was equipped with two micro dispensing units known from T3DP^{18,19,20,31,32}, which allow the deposition of single droplets to close the insufficient filled volumes as well as the manufacturing of finer structures (**Figure 14 and 15**).

Geometrical restrictions of the part complexity or resolution are strongly dependent on the printer setup the continuous material flow as well as the used slicing software. The design rules and the resulting part appearance are at most found to be similar to using FFF of plastics.

Disclosures

The authors have nothing to disclose.

Acknowledgements

This project has received funding from the European Union's Horizon 2020 Research and Innovation Programme under Grant Agreement No 678503.

References

1. ISO/ASTM 52900:2015(en): *Additive manufacturing - General principles - Terminology*. (2015).
2. Lakshminarayan, U., Ogyrdziak, S., Marcus, H.L. Selective laser sintering of ceramic materials. *Proceedings of Solid Free-Form Symposium*. Austin, Texas, USA, 16-26 (1990).
3. Lauder, A., Cima, M.J., Sachs, E., Fan, T. Three dimensional printing: Surface finish and microstructure of rapid prototyped components. *Materials Research Society Symposium Proceedings*. **249**, 331-336 (1992).
4. Chartier T., Badev, A. Rapid Prototyping of Ceramics. In *Handbook of Advanced Ceramics*. Elsevier, 2nd ed., Somiya, S., Elsevier Inc., Oxford, UK (2013).
5. Travitzky, N., et al. Additive Manufacturing of ceramic-based material. *Advanced Engineering Materials*. **16**, 729-754 (2014).
6. Zocca, A., Colombo, P., Gomes, C. M., Günster, J. Additive Manufacturing of Ceramics: Issues, Potentialities, and Opportunities. *Journal of the American Ceramic Society*. **98** (7), 1983-2001 (2015).
7. Felzmann, R., Gruber, S., Mitteramskogler, G., Tesavibul, P., Boccaccini, A.R., Liska, R., Stampfl, J. Lithography-based additive manufacturing of cellular ceramic structures. *Advanced Engineering Materials*. **14**, 1052-1058 (2012).
8. Fischer, U. K., et al. *Lichthärtende Keramikschricker für die stereolithographische Herstellung von hochfesten Keramiken*. (light curing ceramic suspensions for stereolithography of high-strength ceramics), European patent EP 2404590A1 (2012).
9. Homa, J. Rapid Prototyping of high-performance ceramics opens new opportunities for the CIM industry. *Powder Injection Moulding International*. **6** (3), 65-68 (2012).
10. *Admatec unveils ADMAFLEX 130 high performance ceramic 3D printer*. available online: <http://www.3ders.org/articles/20160502-admatec-unveils-admaflex-130-high-performance-ceramic-3d-printer.html> (2016).
11. *France's 3DCeram partners with Japanese firm Sinto to expand ceramic 3D printing in Asia and US*. available online: <https://www.3ders.org/articles/20171006-frances-3dceram-partners-with-japanese-firm-sinto-to-expand-ceramic-3d-printing-in-asia-and-us.html> (2017).
12. Scheithauer, U., et al. CerAMufacturing - Development of ceramic and multi-material components by additive manufacturing methods for personalized medical products. *3D printing in Medicine* **2** (1) (2017).
13. Kieback, B., Neubrand, A., Riedel, H. Processing techniques for functionally graded materials. *Materials Science and Engineering - A*. **362** (1-2), 81-106 (2003).
14. Scheithauer, U., et al. Ceramic-Based 4D Components: Additive Manufacturing (AM) of Ceramic-Based Functionally Graded Materials (FGM) by Thermoplastic 3D Printing (T3DP). *Materials*. **10** (12), 1368 (2017).
15. Moritz, T., et al. Material- and process hybridization for multifunctional ceramic and glass components. *Ceramic Applications*. **5** (2), 66-71 (2017).
16. Scheithauer, U., Schwarzer, E., Moritz, T., Michaelis, A. Additive Manufacturing of ceramic heat exchanger - Opportunities and limits of the Lithography-based Ceramic Manufacturing (LCM). *Journal of Materials Engineering And Performance: Design, Process, Characterization, Evaluation*. **27** (1), 14-20 (2018).
17. Schwarzer, E., Götz, M., Markova, D., Stafford, D., Scheithauer, U., Moritz, T. Lithography-based ceramic manufacturing (LCM) - Viscosity and cleaning as two quality influencing steps in the process chain of printing green parts. *Journal of the European Ceramic Society*. **37** (16), 5329-5338 (2017).
18. Scheithauer, U., Schwarzer, E., Richter, H.J., Moritz, T. Thermoplastic 3D Printing - An Additive Manufacturing Method for Producing Dense Ceramics. *Journal of Applied Ceramic Technology*. **12** (1), 26-31 (2014).
19. Scheithauer, U., Bergner, A., Schwarzer, E., Richter, H.-J., Moritz, T. Studies on thermoplastic 3D printing of steel-zirconia composites. *Journal of Materials Research*. **29** (17), 1931 - 1940 (2014).
20. Scheithauer, U., et al. Additive Manufacturing of Metal-Ceramic-Composites by Thermoplastic 3D-Printing. *Journal of Ceramic Science and Technology*. **06** (02), 125-132 (2015).
21. Agarwala, M.K., et al. Filament Feed Materials for Fused Deposition Processing of Ceramics and Metals. In: *Proceedings of the Solid Freeform Fabrication Symposium*. Volume 7. Bourell, D.L., Beaman, J.J., Marcus, H.L., Crawford, R.H., & Barlow, J.W. (eds) (1996).
22. Kukla, C., et al. Fused Filament Fabrication (FFF) of PIM Feedstocks. In: *Actas del VI Congreso Nacional de Pulvimetalurgia y I Congreso Iberoamericano de Pulvimetalurgia 2017*, 1st ed. Herranz, G., Ferrari, B., & Cabrera, J.M. (eds). Asociación ManchaArte, 1-6 (2017).
23. Agarwala, M.K., et al. Structural Ceramics by Fused Deposition of Ceramics. In: *Proceedings of the Solid Freeform Fabrication Symposium*. (1995).
24. Agarwala, M.K., et al. Fused Deposition of Ceramics and Metals: An Overview. In: *Proceedings of the Solid Freeform Fabrication Symposium*. Bourell, D.L., Beaman, J.J., Marcus, H.L., Crawford, R.H., & Barlow, J.W. (eds) (1996).
25. Onagoruwa, S., Bose, S., & Bandyopadhyay, A. Fused Deposition of Ceramics (FDC) and Composites. In: *Proceedings of the Solid Freeform Fabrication Symposium*. Bourell, D.L., Beaman, J.J., Crawford, R.H., Marcus, H.L., Wood, K.L., & Barlow, J.W. (eds) (2001).
26. McNulty, T.F., Shanefield, D.J., Danforth, S.C., & Safari, A. Dispersion of Lead Zirconate Titanate for Fused Deposition of Ceramics. *Journal of the American Ceramic Society*. **82** (7), 1757-1760 (1999).
27. Mutsuddy, B.C., & Ford, R.G. *Ceramic injection moulding*. Chapman & Hall, London (1995).
28. Edirisinghe, M.J., & Evans, J.R.G. Compounding Ceramic Powders Prior to Injection Moulding. *Proceedings of the British Ceramic Society*. **38**, 67-80 (1986).
29. Suri, P., et al. Effect of mixing on the rheology and particle characteristics of tungsten-based powder injection molding feedstock. *Materials Science and Engineering: A*, **356**, 1-2, 337-344 (2003).
30. Venkataraman, N., et al. Mechanical and Rheological Properties of Feedstock Material for Fused Deposition of Ceramics and Metals (FDC and FDMet) and their Relationship to Process Performance, *Proceedings of the Solid Freeform Fabrication Symposium 1999*. Austin, Texas, USA, 9-11 (1999).

31. Scheithauer, U., *et al.* Investigation of Droplet Deposition for Suspensions Usable for Thermoplastic 3D Printing (T3DP). *Journal of Materials Engineering and Performance*, **27** (1), 44-51 (2017).
32. Weingarten, S., *et al.* Multi-material Ceramic-Based Components - Additive Manufacturing of black-and-white Zirconia Components by Thermoplastic 3D-Printing (T3DP). *Journal of Visual Experiments*, in press (2018).